Diode fibres for fabric–based optical communications

Michael Rein[1,2,3], Valentine Dominique Favrod[1,4], Chong Hou[2,3], Tural Khudiyev[2,3], Alexander Stolyarov[5], Jason Cox[6], Chia-Chun Chung[6], Chhea Chhav[6], Marty Ellis[7], John Joannopoulos[2,3,8] & Yoel Fink[1,2,3,6]*

Semiconductor diodes are basic building blocks of modern computation, communications and sensing[1]. As such, incorporating them into textile-grade fibres can increase fabric capabilities and functions[2], to encompass, for example, fabric-based communications or physiological monitoring. However, processing challenges have so far precluded the realization of semiconducting diodes of high quality in thermally drawn fibres. Here we demonstrate a scalable thermal drawing process of electrically connected diode fibres. We begin by constructing a macroscopic preform that hosts discrete diodes internal to the structure alongside hollow channels through which conducting copper or tungsten wires are fed. As the preform is heated and drawn into a fibre, the conducting wires approach the diodes until they make electrical contact, resulting in hundreds of diodes connected in parallel inside a single fibre. Two types of in-fibre device are realized: light-emitting and photodetecting p–i–n diodes. An inter-device spacing smaller than 20 centimetres is achieved, as well as light collimation and focusing by a lens designed in the fibre cladding. Diode fibres maintain performance throughout ten machine-wash cycles, indicating the relevance of this approach to apparel applications. To demonstrate the utility of this approach, a three-megahertz bi-directional optical communication link is established between two fabrics containing receiver–emitter fibres. Finally, heart-rate measurements with the diodes indicate their potential for implementation in all-fabric physiological-status monitoring systems. Our approach provides a path to realizing ever more sophisticated functions in fibres, presenting the prospect of a fibre 'Moore's law' analogue through the increase of device density and function in thermally drawn textile-ready fibres.

Efforts to increase fibre functions can lead to substantial advantages because the inherent scalability of textile production can be harnessed to produce functional fabrics at a large scale[3,4]. The preform-to-fibre drawing process has been demonstrated to deliver considerable functional capabilities on the fibre and textile level through the incorporation of materials with disparate electronic and optical properties into monofilaments[4–10]. Nevertheless, this process has been limited to materials that could be co-drawn[10] in their viscous states and are typically inferior in performance to 'device-grade' materials that are made using wafer-based approaches[11,12]. In this work, we combine scalable preform-to-fibre drawing with high-performance prefabricated semiconductor devices. Specifically, we incorporate functional semiconductor devices and electrical conductors into a polymer-clad preform, where the viscous polymer cladding simultaneously facilitates device packaging and electrical connectorization in situ during the thermal draw. This process enables new fibre and textile optical communication functionality at unprecedented data rates, as well as a viable path to introducing a gamut of alternative electronic devices into thermally drawn fibres.

The fabrication approach used to produce these fibres is illustrated in Fig. 1a, b. Prefabricated semiconductor devices are embedded in prescribed locations along the preform. As the preform is thermally drawn, the diodes separate axially while their lateral position is preserved by the surrounding viscous polymer. During the drawing process, electrical conductors are unspooled into hollow channels flanking the diodes. The lateral separation of these wires is gradually reduced in the neck-down region until electrical contact is made with the devices. In contrast with previously reported work, where low-melting-temperature metals were thermally co-drawn in polymer fibres[5,10,13], this work demonstrates the ability to embed high-melting-temperature tungsten or copper metallic wires in the fibres during the draw, thus providing highly conductive electrical conduits for the devices. It is worth noting that neither the wires nor the diodes scale down in size during the draw, nor they are in contact with each other in the preform. The preform design and the drawing process itself facilitate the electrical connection between the wires and the devices, as shown in Fig. 1b, c.

Fibres produced using this approach result in a linear array of semiconductor devices uniformly spaced along the fibre length and electrically connected in parallel, with fibre size as small as $350\,\mu m \times 350\,\mu m$. Electrical connection to the in-fibre electrodes is achieved by stripping away the polymer cladding at one end of the fibre. When a voltage is applied to the embedded wires, the in-fibre light-emitting diodes (LEDs) emit light, as shown in Fig. 2a for several fibre samples containing LEDs of different colour. This discovery is the first demonstration of a thermally drawn fibre with embedded semiconductor devices that are able to emit light when the fibre is supplied with electrical current, circumventing the necessity of applying external coatings or conductors[14–20]. Moreover, unlike other[17–20] approaches that yield short fibre lengths, the current approach enables kilometres of functional fibre to be drawn from a single preform with more than a hundred discrete devices connected in parallel throughout the entire fibre. The linear device density in the fibres can be directly controlled by varying the linear density of devices in the preform (for a given preform-to-fibre draw-down ratio) or by introducing several layers of devices and wires in the preform, as demonstrated in Extended Data Fig. 1. For example, for a draw-down ratio of 40, we are able to reduce the inter-diode distance from 2 m to approximately 17 cm. Addition of more layers in the preform will potentially lead to even higher device density in the fibres.

This technique is not limited to the incorporation of LEDs into fibres; other electronic devices could be embedded within thermally drawn fibres in a similar fashion. We embedded p–i–n photodetectors into fibres to enable high-bandwidth photodetection, in contrast to amorphous chalcogenide photoresistive materials previously drawn in fibres[10], which have much lower responsivity and bandwidth compared to crystalline semiconductors such as Si, Ge or GaAs. The method used for the introduction of crystalline GaAs semiconducting p–i–n photodiodes is shown in Extended Data Fig. 2. Characterization of the photodetecting fibres was carried out by illuminating them with the red LED fibres. Figure 2e shows a clear rectifying behaviour of the

[1]Department of Materials Science and Engineering, Massachusetts Institute of Technology, Cambridge, MA, USA. [2]Research Laboratory of Electronics (RLE), Massachusetts Institute of Technology, Cambridge, MA, USA. [3]Institute for Soldier Nanotechnologies, Massachusetts Institute of Technology, Cambridge, MA, USA. [4]Department of Materials Science, Swiss Institute of Technology (EPFL), Lausanne, Switzerland. [5]MIT Lincoln Laboratory, Lexington, MA, USA. [6]Advanced Functional Fabrics of America (AFFOA), Cambridge, MA, USA. [7]Inman Mills, Inman, SC, USA. [8]Department of Physics, Massachusetts Institute of Technology, Cambridge, MA, USA. *e-mail: yoel@mit.edu
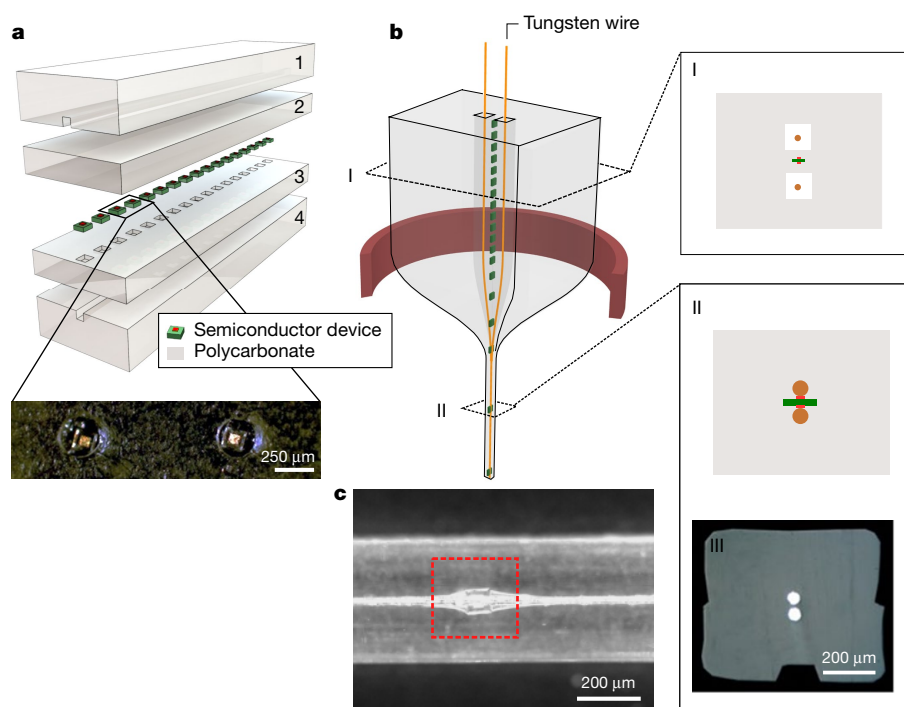
Fig. 1 | Preform structure and fibre drawing results. a, Illustration of the preform structure. It is composed of two main slabs (1 and 4), with a groove milled on their surfaces along the entire length of the preform to accommodate the metallic wires that are interfaced with the devices in the fibre. Numerous pockets with the size of the devices (of the order of 100 μm) are milled in the inner layer (3) to accommodate the electronic devices, as shown in the inset. A top polymeric layer (2) is placed on top of the layer containing the devices, and the preform is thermally consolidated in a heated hydraulic press. **b**, Illustration of the preform drawing process. The metallic wires (orange) are fed through the preform, which is heated and drawn (red ring). The metallic wires and devices are then embedded and packaged in the fibres. Inset I, illustration of the preform cross-section, showing the devices (green rectangle with red contact pads), and wires (orange circles) placed in the grooves (white rectangles). The grooves are larger than the wire in the preform. Inset II, illustration of the fibre cross-section. The devices and wires are well embedded in the fibre cladding, where the wires are touching the contact pads of the devices. Inset III, optical micrograph of the fibre cross-section, showing two tungsten wires embedded in the fibre cladding, without any visible gaps or electrical short-circuiting. **c**, Optical micrograph of the fibre (side view), showing a LED device (inside the dashed red square) and the wires in contact.

photodetecting fibre. In the reverse-bias regime, a substantial increase (about four orders of magnitude) in the photocurrent is observed under illumination compared to the dark current. The measured bandwidth of the photodetecting fibres is shown in Fig. 2f, where the 3-dB bandwidth is found to be 3 MHz—an improvement by orders of magnitude compared to photodetecting fibres based on chalcogenide semiconductors[21]. The limit to the measured bandwidth could be attributed to the parasitic capacitance between the long metallic wires in the fibre. Additionally, the amplifier of the measurement system limits the operation of the system at high frequencies, introducing a trade-off between measured signal strength and system speed.

High-speed fibre LED transmitters and photodetectors present an opportunity for high-bandwidth inter-fibre communication links. Moreover, inter-textile communications functionality is achieved because all components of the fibres are internal to the fibre structure and thus are able to withstand the strains and stresses of textile manufacturing techniques, such as weaving, and even day-to-day handling, including water immersion and machine washing, as shown in Extended Data Figs. 3, 4. Both LED and photodetecting fibres were woven into a separate textile polyester fabric using a conventional industrial loom in a satin weave pattern, as shown in Fig. 3a. Electrical connection to the fibres was made post-weaving at the fabric edge, and the fibres were found to be fully operational. In all cases, the fibres had identical performance as before weaving or the washing cycle tests, presenting a viable path towards the everyday use of this nascent capability.

The opportunity to control the cross-section of the fibre cladding adds an additional degree of freedom to enhance the performance of the fibres. The fibre cross-section can be designed as a lens, with the aim to increase the communication range by collimating and focusing

the light emitted and collected by the LED and photodetecting fibres, respectively. Analytic and numerical simulations were carried out to determine the optimal location of the devices in the fibre, as well as the shape of the cladding, to achieve maximal communication range (see Extended Data Figs. 5–9). This fibre cladding shape is shown in Fig. 3b, c. Experimental results on the effect of the lens cross-section on the communication range are shown in Fig. 3c, where the advantage is apparent for the lensed-cladding fibres compared to fibres with square cross-sections. Both curves follow the inverse-square intensity decay law, as discussed in Methods; nevertheless, shaping the fibre cladding as a collimating lens results in a higher optical flux at the plane of the photodetecting fibre, thus increasing the measured intensity at a given distance.

Integration of high-speed optical transmitters and receivers into fabrics present many compelling applications. First, we demonstrate a fabric-to-fabric communication scheme for two fabrics separated by 1 m in free space, as shown in Fig. 4a, b. Figure 4b shows the signal recorded by the photodetecting fibre when the LED fibre is driven with a frequency of 20 kHz, close to the maximum of the audible frequency range, demonstrating the ability to transmit audio signal over fabric. This capability could be exploited for numerous other applications, from fabric-enabled light fidelity technology[21], to fabric-encrypted local information transfer and indoor positioning platforms. Second, we demonstrate the capabilities of these fibres in the context of physiological measurements. Specifically, we demonstrate a textile-based photoplethysmography system for pulse measurement[22] based on the developed textile platform. Here, a green LED fibre is embedded in a cotton fabric sock adjacent to a GaAs photodetecting fibre, as illustrated in Fig. 4c. A pulse measurement is obtained by placing an index finger on both fibres. The change of the
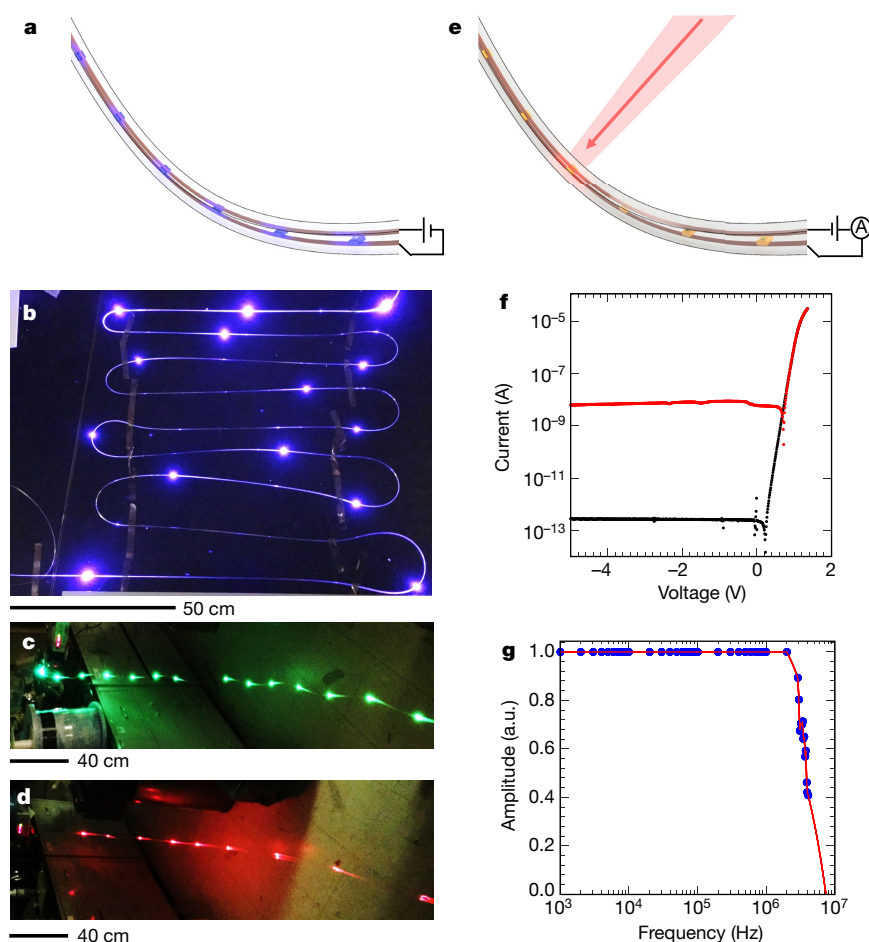
Fig. 2 | Light-emitting and high-bandwidth photodetecting fibres. a–d, Multimaterial fibres with light-emitting functionality. **a**, Illustration of the light-emitting fibres. The wires (orange) are connected to the LEDs (purple) and to a current supply (black lines) at the fibre end. **b**, Photograph of light-emitting fibres containing InGaN blue-colour LEDs. The devices appear every 370 ± 110 mm and the fibres are laid flat on a table. **c**, Fibres containing InGaN LEDs emitting green colour. The fibres were unspooled and held on the other end (right-hand side of the photograph). **d**, Fibres containing AlGaAsP LEDs emitting red colour. The fibres were unspooled and held on the other end (right-hand side of the photograph). **e–g**, High-bandwidth photodetecting fibres. **e**, Illustration of the photodetecting fibre structure, where an individual photodiode (orange) interacts with an external beam of light (red arrow). **f**, Current–voltage curve of a fibre containing one GaAs device, showing a clear rectifying behaviour. The black curve was obtained in darkness and the red curve under illumination. In the reverse-bias regime the current increases by a few orders of magnitude when the fibre is illuminated. The plot shows the absolute value of the current on a logarithmic scale. Application of a logarithmic function on low voltage and current values shows a kink in the response, which is not present in the raw data. **g**, Bandwidth measurement (blue circles) of the photodetecting fibre. The 3 dB bandwidth achieved is around 3 MHz. a.u., arbitrary units. The red line is a guide for the eye.

measured light intensity recorded by the photodetecting fibre due to the change in the light reflectance from the skin is shown in Fig. 4d. The measured signal directly correlates with volume changes in small blood vessels, which expand and constrict with every heartbeat. These results demonstrate the potential to integrate physiological sensors fully within fibres and textiles, not as add-ons to fabrics. The results presented here demonstrate a new paradigm for integrating pre-fabricated high-performance semiconductor devices into a fibre form factor, paving the way towards increasingly functional fibre and fabric systems. We envision that this technology will enable new technological advances in the textile and apparel domains, telecommunications, as well as in biological and medical sciences. In particular, multifunctional fibres could enable a new generation of optigenetically modified neuron fibre probes[23], active media for textile–bacteria interaction[24] systems or active textiles with fragrance- or medicine-release capabilites[25].
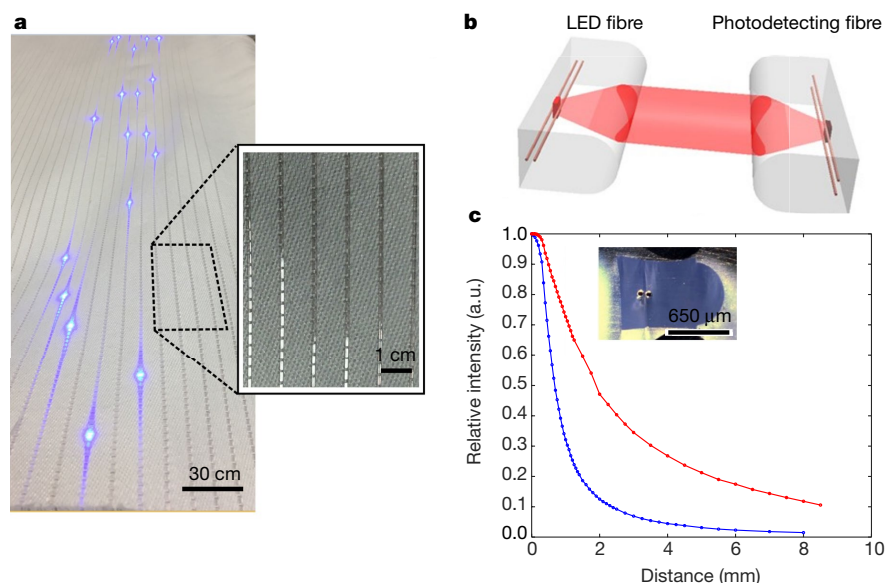

Fig. 3 | Embedding of fibres in fabrics and light collimation by the fibre cladding. a, Light-emitting and photodetecting fibres embedded in a fabric. The blue-colour light-emitting fibres are embedded in a fabric and in operation. Inset, a closer look at the fibre–fabric interface. **b**, Communication between two lensed fibres. Left fibre, light-emitting fibre; right fibre, photodetecting fibre; red-shaded area, emitted light. The fibre lens could be considered as a cylindrical lens extending along the whole length of the fibre. **c**, Measured current of the photodetecting fibre, normalized with respect to the current measured at a contact between fibres, as a function of the distance between fibres. Blue symbols, no collimation or focusing; red symbols, light collimation and light focusing on the photodiode; blue and red lines, guides for the eye. Inset, optical micrograph of the light-emitting fibre, showing the lens and the two tungsten wires embedded in the cladding.
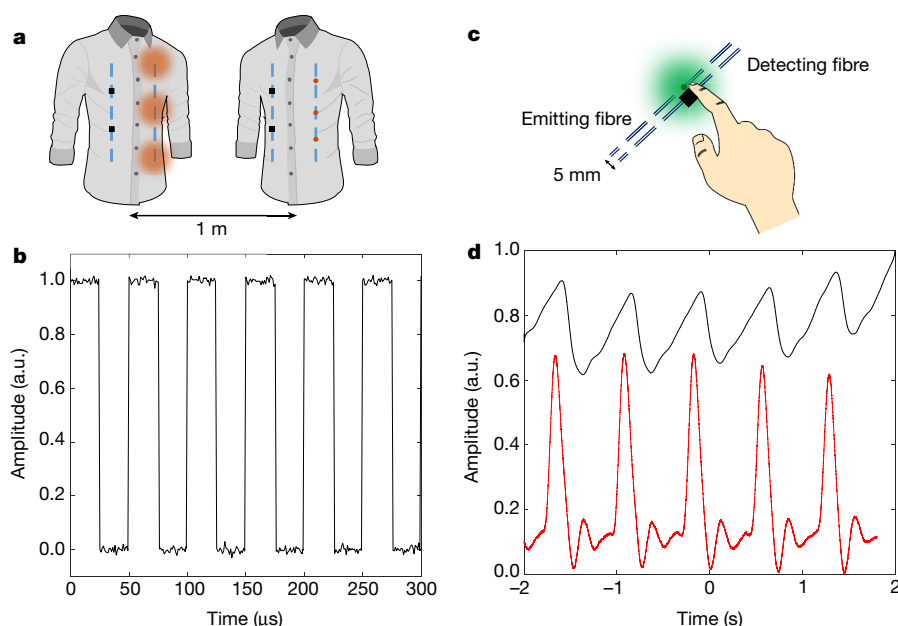
Fig. 4 | Applications of light-emitting and light-detecting fabric.
a, Illustration of bi-directional communication system concept. A garment is composed of a fabric that contains both light-emitting (light blue dashed line with red circles) and photodetecting (light blue dashed line with black squares) fibres. The light-emitting fibres are modulated to transmit information that is being recorded by the photodetecting fibres in the other garment, placed at a distance of 1 m from each other. **b**, Experimental results of the current recorded by the photodetecting fibres incorporated into a fabric. The light was emitted from LED fibres embedded in another fabric located at a distance of 1 m from the photodetecting fabric. The light-emitting fibres were connected to a function generator delivering a square-wave signal with a frequency of 20 kHz. The transmission of the signal was recorded by the fibres (see Methods for additional details). **c**, Illustration of a photoplethysmography pulse measurement setup using light-emitting (dashed line with green light) and photodetecting (dashed line with black square) fibres placed at a distance of 5 mm from each other. Placing a finger on both fibres allows recording the reflected light, which is sensitive to blood circulation in the blood vessels close to the skin. **d**, Experimental results of the current measured by the photodetecting fibre (black curve) compared to the output of a commercial pulse sensor (red curve). Periodic changes in the recorded intensity correspond to the frequency of the pulse.

Online content
Any Methods, including any statements of data availability and Nature Research reporting summaries, along with any additional references and Source Data files, are available in the online version of the paper at https://doi.org/10.1038/s41586-018-0390-x.

1. Kitai, A. in *Principles of Solar Cells, LEDs and Diodes: The Role of the PN Junction* Chs. 2, 5 (John Wiley & Sons, Chichester, 2011).
2. Stoppa, M. & Chiolerio, A. Wearable electronics and smart textiles: a critical review. *Sensors* **14**, 11957–11992 (2014).
3. Abouraddy, A. F. et al. Towards multimaterial multifunctional fibres that see, hear, sense and communicate. *Nat. Mater.* **6**, 336–347 (2007).
4. Tao, G., Abouraddy, A. F., Stolyarov, A. M. & Fink, Y. in *Lab-on-Fiber Technology* (eds Cusano, A. et al.) 1–26 (Springer International Publishing Switzerland, 2015).
5. Gumennik, A. et al. All-in-fiber chemical sensing. *Adv. Mater.* **24**, 6005–6009 (2012).
6. Lestoquoy, G., Chocat, N., Wang, Z., Joannopoulos, J. D. & Fink, Y. Fabrication and characterization of thermally drawn fiber capacitors. *Appl. Phys. Lett.* **102**, 152908 (2013).
7. Hart, S. D. et al. External reflection from omnidirectional dielectric mirror fibers. *Science* **296**, 510–513 (2002).
8. Chocat, N. et al. Piezoelectric fibers for conformal acoustics. *Adv. Mater.* **24**, 5327–5332 (2012).
9. Egusa, S. et al. Multimaterial piezoelectric fibres. *Nat. Mater.* **9**, 643–648 (2010).
10. Bayindir, M. et al. Metal–insulator–semiconductor optoelectronic fibres. *Nature* **431**, 826–829 (2004).
11. Rein, M. et al. Self-assembled fibre optoelectronics with discrete translational symmetry. *Nat. Commun.* **7**, 12807 (2016).
12. Borisova, Z. U. *Glassy Semiconductors* (Plenum Press, New York, 1981).
13. Sorin, F., Lestoquoy, G., Danto, S., Joannopoulos, J. D. & Fink, Y. Resolving optical illumination distributions along an axially symmetric photodetecting fiber. *Opt. Express* **18**, 24264–24275 (2010).
14. Cherenack, K. H., Kinkeldei, T., Zysset, C. & Troster, G. Woven thin-film metal interconnects. *IEEE Electron Device Lett.* **31**, 740–742 (2010).
15. Cherenack, K., Zysset, C., Kinkeldei, T., Münzenrieder, N. & Tröster, G. Woven electronic fibers with sensing and display functions for smart textiles. *Adv. Mater.* **22**, 5178–5182 (2010).
16. Dias, T. & Ratnayake, A. in *Electronic Textiles* 109–116 (Woodhead Publishing, Cambridge, 2015).
17. Kwon, S. et al. High luminance fiber-based polymer light-emitting devices by a dip-coating method. *Adv. Electron. Mater.* **1**, 1500103 (2015).
18. Zhang, Z. et al. A colour-tunable, weavable fibre-shaped polymer light-emitting electrochemical cell. *Nat. Photon.* **9**, 233–238 (2015).
19. O'Connor, B., An, K. H., Zhao, Y., Pipe, K. P. & Shtein, M. Fiber shaped light emitting device. *Adv. Mater.* **19**, 3897–3900 (2007).
20. O'Connor, B., Pipe, K. P. & Shtein, M. Fiber based organic photovoltaic devices. *Appl. Phys. Lett.* **92**, 2006–2009 (2008).
21. Dimitrov, S. & Haas, H. *Principles of LED Light Communications* (Cambridge University Press, Cambridge, 2015).
22. Allen, J. Photoplethysmography and its application in clinical physiological measurement. *Physiol. Meas.* **28**, R1–R39 (2007).
23. Canales, A. et al. Multifunctional fibers for simultaneous optical, electrical and chemical interrogation of neural circuits *in vivo*. *Nat. Biotechnol.* **33**, 277–284 (2015).
24. Levskaya, A. et al. Engineering *Escherichia coli* to see light. *Nature* **438**, 441–442 (2005).
25. Broichhagen, J. et al. Optical control of insulin release using a photoswitchable sulfonylurea. *Nat. Commun.* **5**, 5116 (2014).

METHODS

Preform fabrication. Two slabs of polycarbonate (PC) (McMaster Carr #1749K149) were milled to introduce a trench running the entire length of the preform (~8 inches; 1 inch = 2.54 cm) with a width of 1.25 mm and depth of 1.6 mm. Two Teflon bars were inserted into milled pockets with similar size to prevent pocket collapse during preform consolidation. A thin, 500-μm-thick PC layer was consolidated on one of the PC slabs in a hydraulic hot press heated to a temperature of 175 °C for 5 min and then water-cooled. Small pockets were drilled in the thin PC layer to accommodate the microelectronic devices. The size of the pockets was slightly larger than that of the devices. The distance between the pockets was varied according to the desired density of the devices in the fibre. The devices were transferred manually to the drilled pockets in the preform while keeping the orientation of each device constant. Multiple devices were successfully integrated, such as LEDs (InGaN blue-colour LEDs, Cree C460UT170-0014-31; InGaN green-colour LEDs, Cree C527UT170-0108-31; AlGaInP red-colour LEDs, Three Five Materials TCO-07UOR), or various photodetectors (GaAs p–i–n photodiodes, Broadcom SPD2010; Si photodiodes, Three Five Materials PD-30027A-B). Another thin, 0.5-mm-thick layer was consolidated on top of the diodes to hold them in place in the preform. The top PC slab was consolidated on top of the layers to form the full preform. The final consolidation was performed in a hydraulic hot press at a temperature of 175 °C for an hour, and then the preform was slowly cooled to room temperature.

Fibre drawing. The fibres were fabricated by the thermal drawing process by placing the preform in a three-zone heating furnace, where the top, middle and bottom zones were heated to 150 °C, 270 °C and 110 °C, respectively. The preform was fed into the furnace at a rate of 1 mm min^{-1} and drawn at a speed of 1.6 m min^{-1}, which resulted in a draw-down ratio of 40. Multiple tungsten (Goodfellow #343-809-07) or copper (Goodfellow #271-974-11) wires with a diameter of 50 μm were continuously fed into the preform during the draw. The pockets that accommodated the diodes and the wires in the fibre were smaller than the non-melting components, enabling full encapsulation of both the devices and the wires in the polymeric cladding; they also induced incision into the thin PC layers, which resulted in electrical connection between the wires and the terminals of the electronic devices. Away from the electronic devices, the PC layer was still present, and no short-circuiting occurred between the wires. Hundreds of metres of fibre was collected from each draw.

Optical microscopy characterization. To obtain the cross-section micrographs, the fibres were placed in a plastic holder (Struers Multiclips) and encapsulated in an epoxy matrix (Struers EpoFix), which was subsequently polished. The optical micrographs were obtained using a stereoscope microscope (Nikon SMZ745T).

Occasionally, some small air pockets could be observed around the devices after the draw. In most cases, these pockets did not interfere with the operation of the devices, as they were anchored in the surrounding polymeric cladding.

Operation of light-emitting fibres. The electrical wires in the fibre were exposed from the cladding by cutting the soft PC cladding. The exposed tungsten or copper wires were connected to a diode driver (Thorlabs LDC205C) and the current was supplied by the instrument, up to 30 mA for each light-emitting device.

Crystalline photodetectors characterization. To obtain the IV characteristics, the photodetecting fibres were connected to a power supply and pico-ammeter measurement system (Keithley 6487/6517A). The measurement was made in the dark and under illumination by a red light-emitting fibre placed at a distance of 10 mm from the photodetecting fibre. The operational bandwidth of the fibre photodetecting devices was measured using a function generator (Tektronix AFG3252) connected to a fibre pigtailed laser diode (Thorlabs LPM-660-SMA), configured as the illumination source. The electrical conductors of the photodetecting fibre were connected to a trans-impedance amplifier (Thorlabs TIA60) and to an oscilloscope (Agilent Technologies DSOX - 3014A). The frequency of the laser diode illumination swept a range of frequencies as the amplitude of the photodiode device voltage was measured with the oscilloscope at each frequency point.

Weaving fibres into textiles. The weaving of the fabric was carried out using a Picanol Gamma rapier weaving machine. In the warp direction, a satin weave design was used, and the yarn component was a blend of conventional nylon and cotton with a density of 100 threads per inch. In the weft direction, conventional filament polyester was used between the functional fibres at a density of 35 threads per inch. Device fibres were introduced into the fabric only in the weft direction. Although we did not measure the tensile force acting on the fibres during the process, later studies showed that the fibres can withstand tensile stress up to 70 MPa. We assume that the fibres should survive the weaving process as long as the tensile stress is kept under 70 MPa.

Information transmission from fabric to fabric. Red-light-emitting fibres were woven into a fabric, while Si photodetecting fibres were woven into a second fabric. The light-emitting fibres were connected to a function generator, and the photodetecting fibres were connected to a custom-built trans-impedance circuit, with the output of the circuit connected to an oscilloscope. The light-emitting fibre was

driven by a square wave (alternating voltage of 5 V) with a frequency of 20 kHz that electrically drove three devices per fibre, emitting a total optical power of 90 mW. The photodetecting fabric (with one photodetector embedded in each fibre) was placed at a distance of 1 m from the light-emitting fabric and obtained a signal that was recorded.

Photoplethysmography measurements. A green-light-emitting fibre was placed at a distance of 5 mm from a photodetecting fibre containing a GaAs detector. The light-emitting fibre was connected to a continuous current supply (Thorlabs LDC205C) and driven with a current of 20 mA. The photodetecting fibre was connected to a low-pass filter and the pulse measurement trace was collected with a computerized oscilloscope (Cleverscope CS328A) when a finger was placed on both fibres.

Device density control in the fibres. The linear device density in the fibres can be directly controlled by varying their linear density in the preform ($\Delta l_{preform}$) and by varying the draw-down ratio (β), as demonstrated in Extended Data Fig. 1. The draw-down ratio is a ratio between the diameter of the preform ($d_{preform}$) and the diameter of the resulting fibre (d_{fibre}) and is described by the relation $\beta = d_{preform}/d_{fibre} = \sqrt{v_{draw}/v_{feed}}$, where v_{draw} is the fibre drawing speed and v_{feed} is the preform feed speed. According to the law of mass preservation, the axial distance in the preform will be translated to an axial distance in the fibre according to the relation $\Delta l_{fibre} = \beta^2 \Delta l_{preform}$. Thus, to decrease the inter-diode distance, we can vary the distance between the diodes in the preform or decrease the draw-down ratio.

For example, for a draw-down ratio of 40 and a linear device separation of 1.25 mm in the preform, the diodes in the fibre appear every 2,000 ± 110 mm. To increase the device density in the fibres, we can place them adjacent to each other in the preform, as demonstrated in inset (ii) of Extended Data Fig. 1b, and obtain a fibre with an inter-diode spacing of 370 ± 100 mm. The device dimensions set an upper limit on the highest linear device density that can be achieved in a fibre when the devices are placed in a straight line in the preform for a given draw-down ratio. To further increase the device density, these could be placed in several layers in the preform. This concept was demonstrated for two layers stacked vertically with a common anode wire, as shown in Extended Data Fig. 1c. The draw of this preform with the same draw-down ratio of 40 yields a fibre with an inter-diode separation of 173 ± 92 mm, increasing the effective linear density of the devices by a factor of two compared to a single device layer. Addition of more layers vertically or horizontally in the preform will potentially lead to a higher device density in the fibres. The measured dispersion in the device location is due to the finite precision of the positioning of the devices in the preform, which does not change when increasing the device density in the preform.

Extended Data Fig. 1d, e presents the effect of the inter-diode distance in the preform and the draw ratio on the distance between devices in the fibres, respectively. The effect of increasing the number of diode layers in the preform is demonstrated as well.

Increasing the communication range. An experiment was carried out to determine the dependence of the signal strength transmitted between a light-emitting fibre and a photodetecting fibre on the distance between the two fibres, as demonstrated in Extended Data Fig. 5. The figure shows that the recorded photocurrent is inversely proportional to the distance squared for distances larger than 1 mm. For shorter distances, the intensity decay diverges from this dependence owing to the finite size of the emitter and detector as well as the Lambertian radiation pattern of the LED. This intensity decay will affect the maximal communication distance, mostly because any signal below 0.1 nA is comparable to the ambient background noise in the experimental environment. This requires amplifying the signal. To increase the communication range substantially, a few approaches could be undertaken: (1) Increase the emitter intensity or reduce the beam divergence; (2) increase the receiver aperture size and photoelectric responsivity; (3) use appropriate electronic circuitry to measure the current output from the fibres.

Unfortunately, a larger device size means a larger fibre size—this is not desired because it makes the fibre stiffer, complicating the subsequent weaving process to integrate the fibres into fabrics. Higher illumination intensities lead to higher heat released from the semiconducting devices, causing them to heat to elevated temperatures and eventually melt the fibre cladding that encapsulates them. The electrical circuitry connected to the photodetecting fibre also influences the communication range. Amplifying the signal with high-gain circuitry will increase the communication range at the expense of noise amplification and operational bandwidth of the system. Alternatively, to increase the range of communication, the external shape of the fibre cladding could be optimized to collimate the light emitted from the light-emitting fibre and to focus the light on the photodetecting fibre, effectively introducing a cylindrical lens along the fibre length.

A photodetecting fibre was placed in front of a light-emitting fibre while the photocurrent from the photodetecting fibre was recorded as a function of the distance between the fibres. The results are shown in Extended Data Fig. 5, which demonstrates an inverse-distance-squared dependence at distances larger than

1 mm from the fibres, as expected from theory. Light collimation and focusing are expected to extend the communication range between the fibres. To find the optimal location of the devices in the fibre and the optimal shape of the cladding, a two-dimensional ray-optics numerical simulation was carried out. The size of the fibres was set to $500\,\mu m \times 500\,\mu m$. One fibre contained a photodetector (red rectangle, of size $250 \times 250\,\mu m$) and the other fibre contained a finite-size source that emulated the LED. This source emitted light in a hemispherical configuration, with a Lambertian radiation pattern. The simulation was carried out using the ray-tracing module of the COMSOL software. This simulation was used to determine the optimal device location in the fibre and the optimal fibre shape. Adding a curved structure to the fibre surface and placing the device in the focal point of this lens is an effective approach to collimating and focusing the light between the light-emitting and photodetecting fibres. On the basis of lens physics, we should aim to place the devices in the focal point of the lens to both focus an external light source and to collimate the light emitted from the LEDs in the fibre. For a thick lens, the focal distance is given by the lens-maker's equation[26]:

$$\frac{1}{f} = (n-1)\left(\frac{1}{R_1} - \frac{1}{R_2} + \frac{(n-1)t}{nR_1R_2}\right) \qquad (1)$$

Here, f is the focal length of the lens, n is the refractive index of the material of the lens, R_1 and R_2 are the radii of curvature of the two spherical parts of the lens and t is the lens thickness. Because the devices are embedded in the cladding, we have a curved surface only on the external side of the fibre, whereas the other side is flat, that is, with infinite radius. Thus, the focal point of such a lens will be as given by:

$$\frac{1}{f} = \frac{n-1}{R_1} \qquad (2)$$

The cladding of the fibres is made of PC, which has an index of refraction of around $n = 1.58$ in the visible-wavelength domain. This locates the focal point of the fibre at a distance of $1.72R_1$ and defines the desired fibre structure, as shown in Extended Data Fig. 6a. Here we can see that the optimal structure is a rectangular or square fibre, where the device is located approximately $190\,\mu m$ from the square's centre. The square is assumed to have side length of $500\,\mu m$, equal to the lens diameter. We performed a ray-optics simulation to find the optimal location of the device in the fibre, and the ray-tracing results are shown in Extended Data Fig. 6b.

In this figure, we can see that some of the light is collimated by the lens, whereas some light is reflected or not collected by the lens and is allowed to escape the fibre without collimation. Other focusing techniques were considered; for example, using mirrors or multiple lenses on the surface of the fibre. Unfortunately, these geometries are harder to achieve in a fibre, and could be explored in the future. A similar approach was used to find the optimal device location and fibre shape for focusing a collimated beam of light on the photodetector. Extended Data Fig. 7 shows the results of a simulation carried out to determine the optimal location of the device in the fibre for collecting external light. Extended Data Fig. 7a shows the structure of the fibre and Extended Data Fig. 7b, c shows the results of the ray-tracing simulation and the dependence of the intensity on the location of the device in the fibre. We carried out a similar simulation for both types of fibres, one in front of the other, as shown in Extended Data Fig. 8. We can see that adding lenses on both fibres collimates and focuses some of the light, which will potentially extend the communication distance. We have reduced the optimized fibre structure to practice, as shown in Fig. 3c (inset).

Fibre device yield. Multiple optimization steps on the preform structure and drawing process have resulted in a yield of up to 95% (number of LEDs that light up relative to the total number of devices embedded in the preform). The main failure mechanisms observed in the process are misalignment between the metallic wires and the embedded devices, fibre polymer cladding or wire breakage during fibre drawing, lack of contact between the wires and the device contact pads, or occasional short-circuiting between the metallic wires in the fibres. Characterization results of the light-emitting fibres (measurement of the distance between adjacent diodes and of the emitted power) are shown in Extended Data Fig. 9. This characterization was performed on a fibre drawn from a preform containing two parallel rows of diodes, drawn down by a factor of 33. Most of the diodes appear at the expected distance. The power of each diode was measured and normalized with the maximum power emitted by the diode located closest to the driving circuit, which applied a constant voltage of 6 V. The emitted power decreases with the distance from the voltage source owing to the finite wire resistance. We drew more than 30 preforms with various diodes and all our draws yielded sections of working fibres.

Data availability. The data that support the findings of this study are available from the corresponding author upon reasonable request.

26. Hecht, E. *Optics* (Pearson Education, London, 2014).
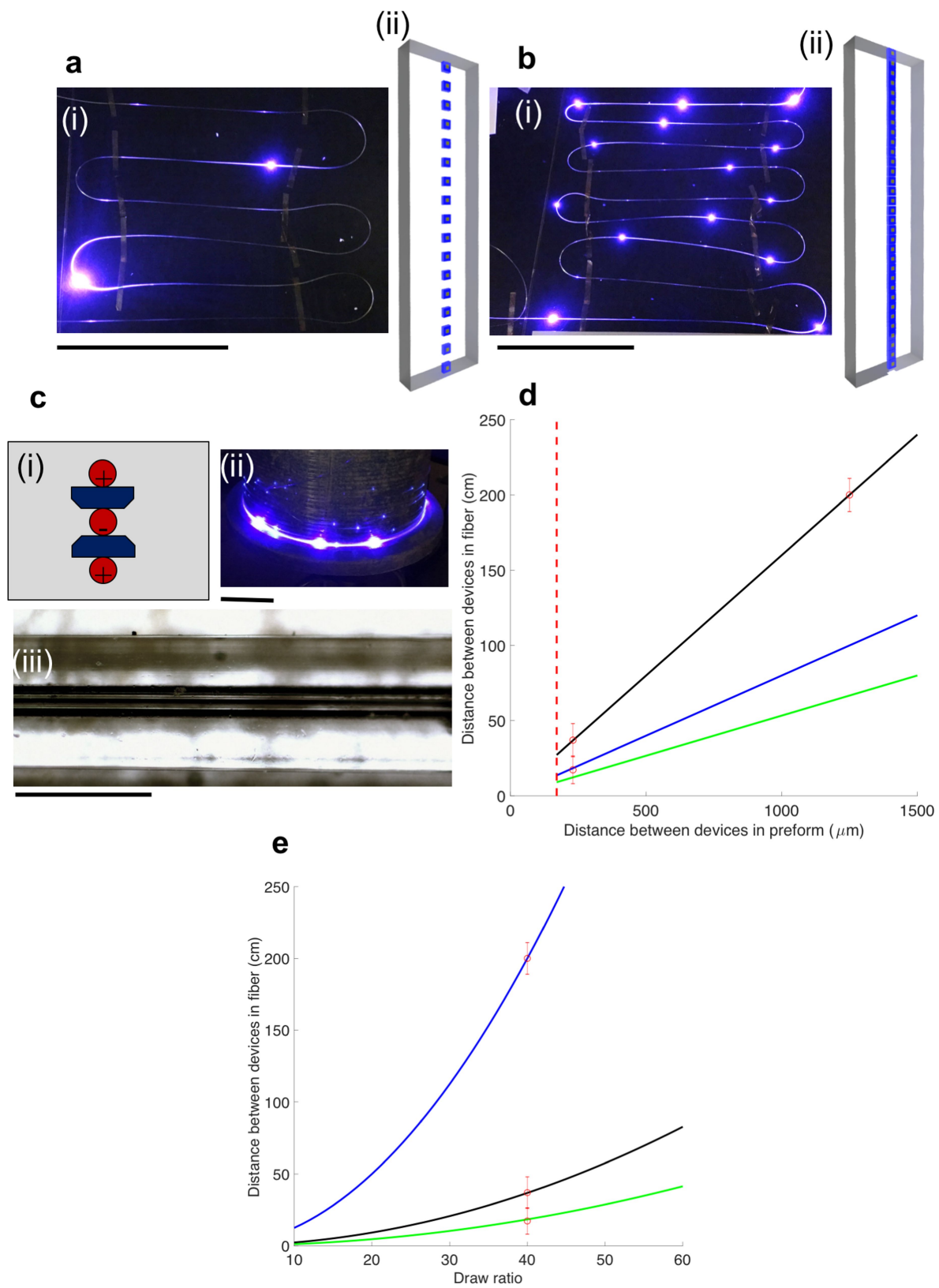
Extended Data Fig. 1 | See next page for caption.

Extended Data Fig. 1 | Controlling device density in light-emitting fibres. a, Light-emitting fibres with low device density. (i) Photograph of light-emitting fibres containing blue-colour LEDs. The devices appear with a periodicity of $2,000 \pm 110$ mm. Scale bar, 50 cm. (ii) Illustration of the device density in the polymeric layer, which is placed in the middle of the preform, with a device separation of 1.25 mm. **b**, Higher density of devices in the fibre. (i) Photograph of light-emitting fibres containing blue-colour LEDs, where the devices appear every 370 ± 110 mm. This is the maximum linear density available with the given draw-down ratio (40) and device size for the single-layer (plane) architecture. Scale bar, 50 cm. (ii) Illustration of the maximal linear density of devices in the preform. The devices are placed side by side in a single plane. **c**, An alternative approach to increasing device density in fibres. (i) Illustration of the structure of the fibre cross-section, where light-emitting devices (blue shapes) are placed in two layers on top of each other, connected to metallic electrodes (red circles) for current delivery. The $+$ and $-$ signs represent the polarity of the wires when connected to the power supply.

(ii) Photograph of the resulting fibre, in which the devices appear every 173 ± 92 mm. Scale bar, 20 cm. (iii) Side view of the light-emitting fibre, showing the presence of three electrode wires. Scale bar, 600 μm. **d**, Distance between devices in the fibre as a function of the distance between devices in the preform for a draw-down ratio of 40 and using LEDs. Solid lines show calculation results; black curve, single device layer in the preform; blue curve, two device layers in the preform; green curve, three device layers in the preform. Red circles represent measurements of inter-device spacing in the fibres. The dashed red line corresponds to the minimal distance between devices in the preform, which is equal to the size of the devices (170 μm). **e**, Distance between devices in the fibre as a function of the draw-down ratio. Solid curves show calculation results: black curve, single device layer with a spacing of 230 μm between devices in the preform; green curve, two device layers with a spacing of 230 μm; blue curve, single device layer with a spacing of 1.25 mm. Red circles, measurements of inter-device spacing in the fibres. Error bars represent one standard deviation.
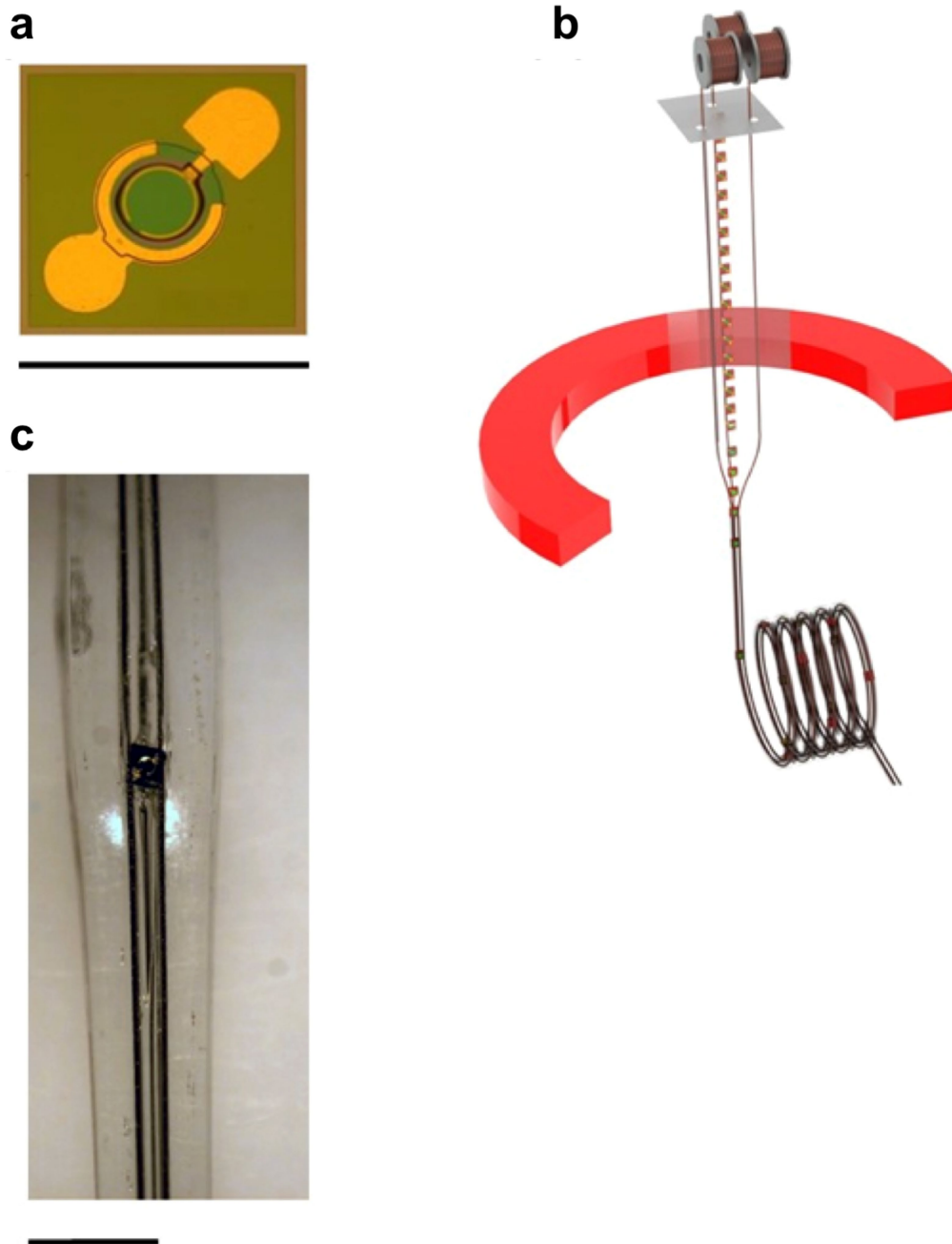
Extended Data Fig. 2 | Drawing of high-bandwidth photodetecting fibre. a, Optical micrograph of a commercial GaAs photodetecting device element. The central part is the device aperture, surrounded by two metallic contacts. Scale bar, 275 μm. **b**, Illustration of the preform drawing process for the photodetecting fibres. The contact to the devices is established on the same side of the detectors, keeping the apertures of the devices uncovered by wires, whereas the third wire is placed behind the devices to prevent them from rotating during fibre drawing. **c**, Optical micrograph of the photodetecting fibres, showing a device embedded in the fibre. Scale bar, 600 μm.
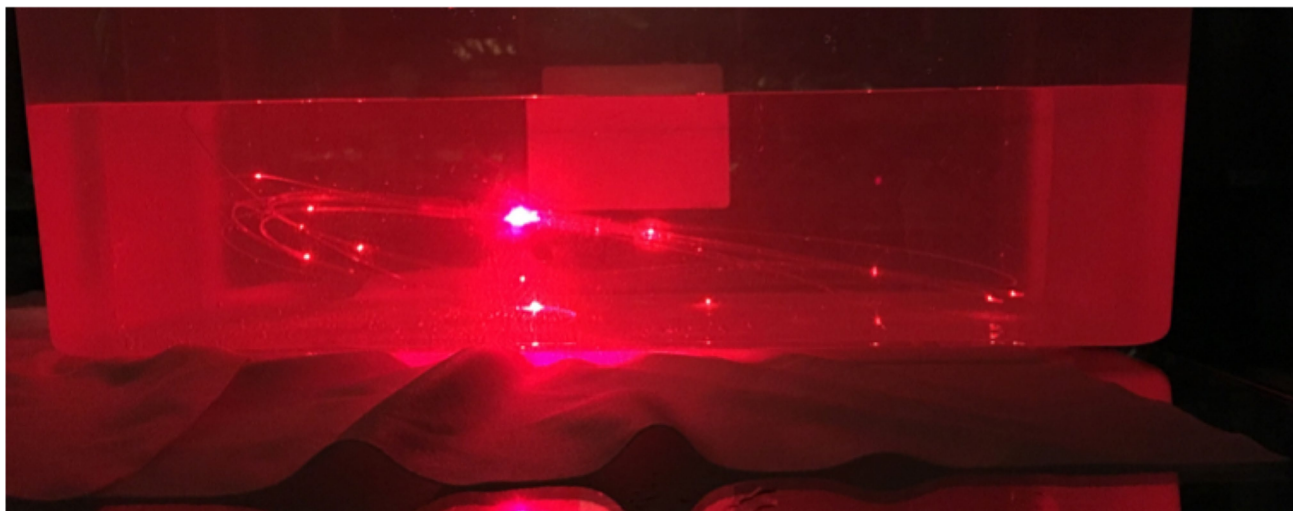
Extended Data Fig. 3 | Photograph of a light-emitting fibre immersed in a tank of water. The fibres are fully operational when immersed in water.
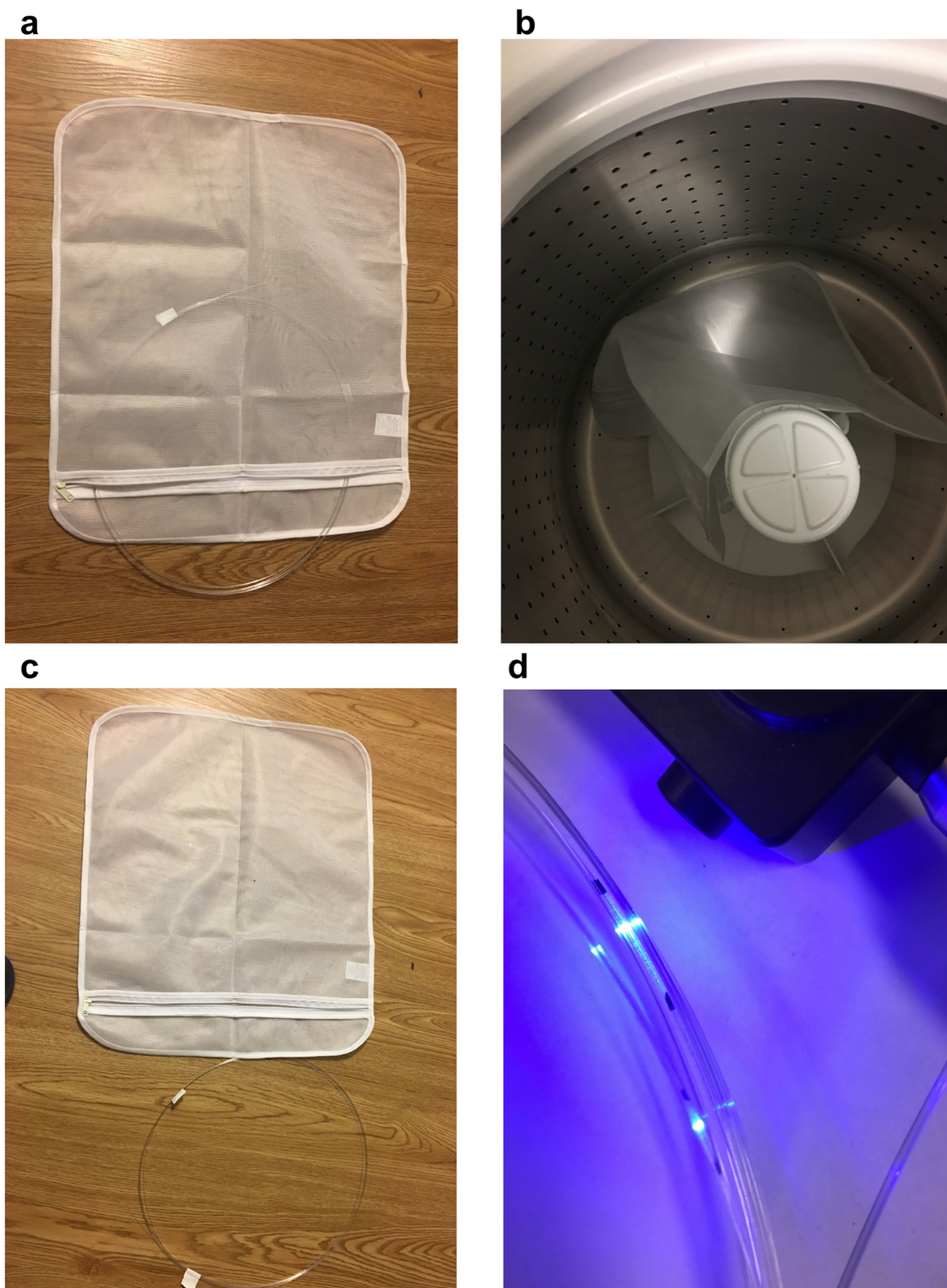
Extended Data Fig. 4 | Machine washing experiments with light-emitting fibres. a, A bunch of light-emitting fibres is placed in a water-permeable protective sack. **b**, The protective sack with the fibres is placed in a household washing machine. **c**, Fibres and sack after a washing cycle. **d**, Fibre operation and light emission after the washing cycle.

a

b

c
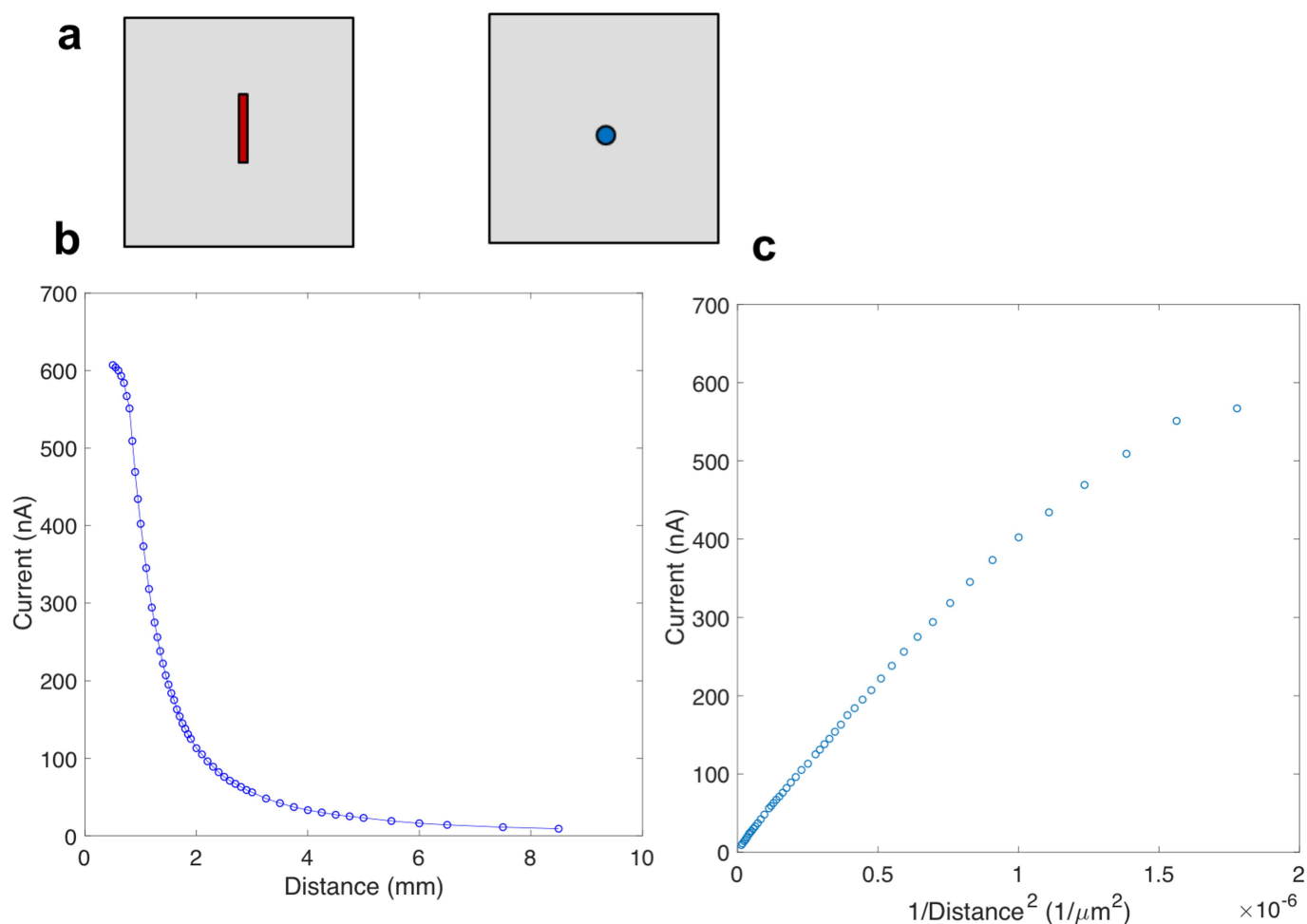
Extended Data Fig. 5 | Measurement of current registered by the photodetecting fibre as a function of the distance between the photoemitting and photodetecting fibres. a, Illustration of the experimental setup. Red rectangle, photodetector; blue circle, LED point source; grey square, PC cladding. **b**, Current registered by the photodetecting fibre versus its distance from the light-emitting fibre, obtained with the photodetecting fibre placed in front of a light-emitting fibre while varying the distance between them. **c**, Current versus the inverse distance squared. The plot shows a linear dependence between the current and the inverse distance squared, which corresponds to the inverse-square law, at distances larger than 1 mm between the fibres. At shorter distances, deviation from the inverse-square law is observed. Several factors could contribute to this deviation, such as the finite sizes of the emitter and detector, the Lambertian profile of the emission and contact between the fibres at lower distances, which may have distorted the distance measurements between the fibres.
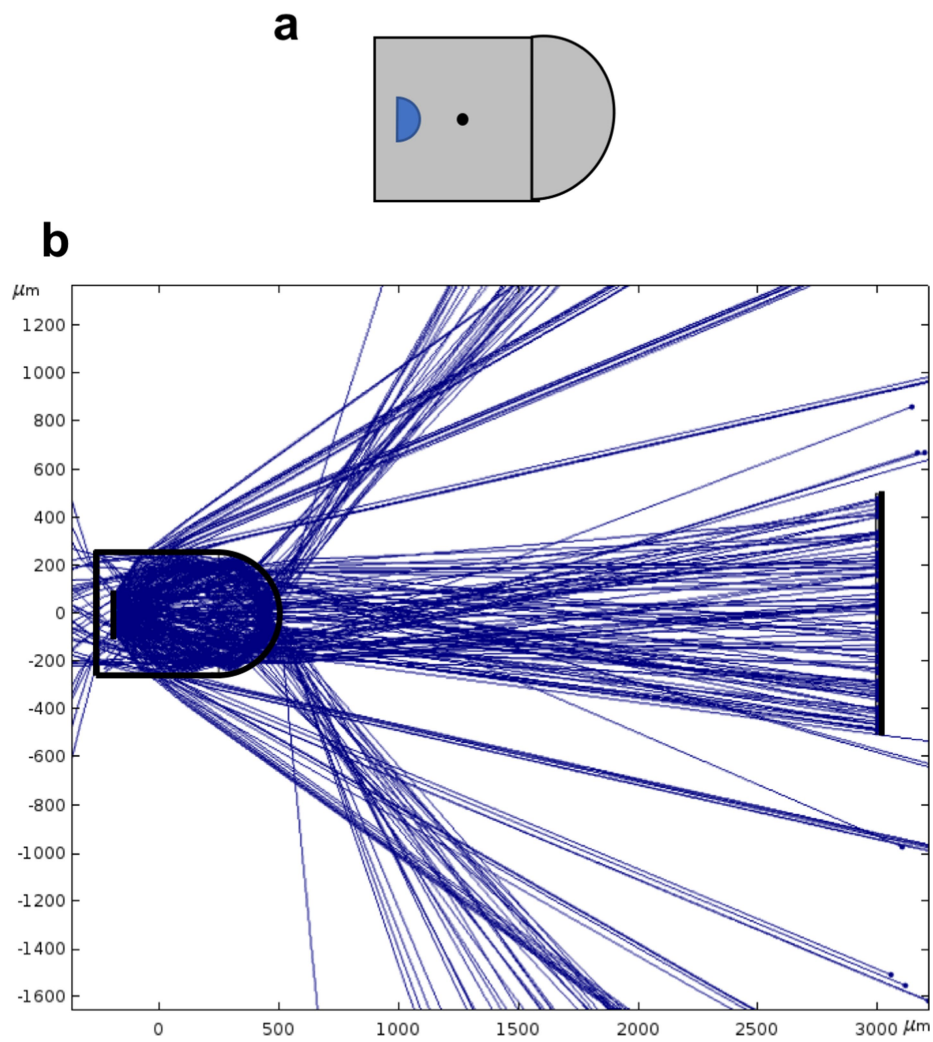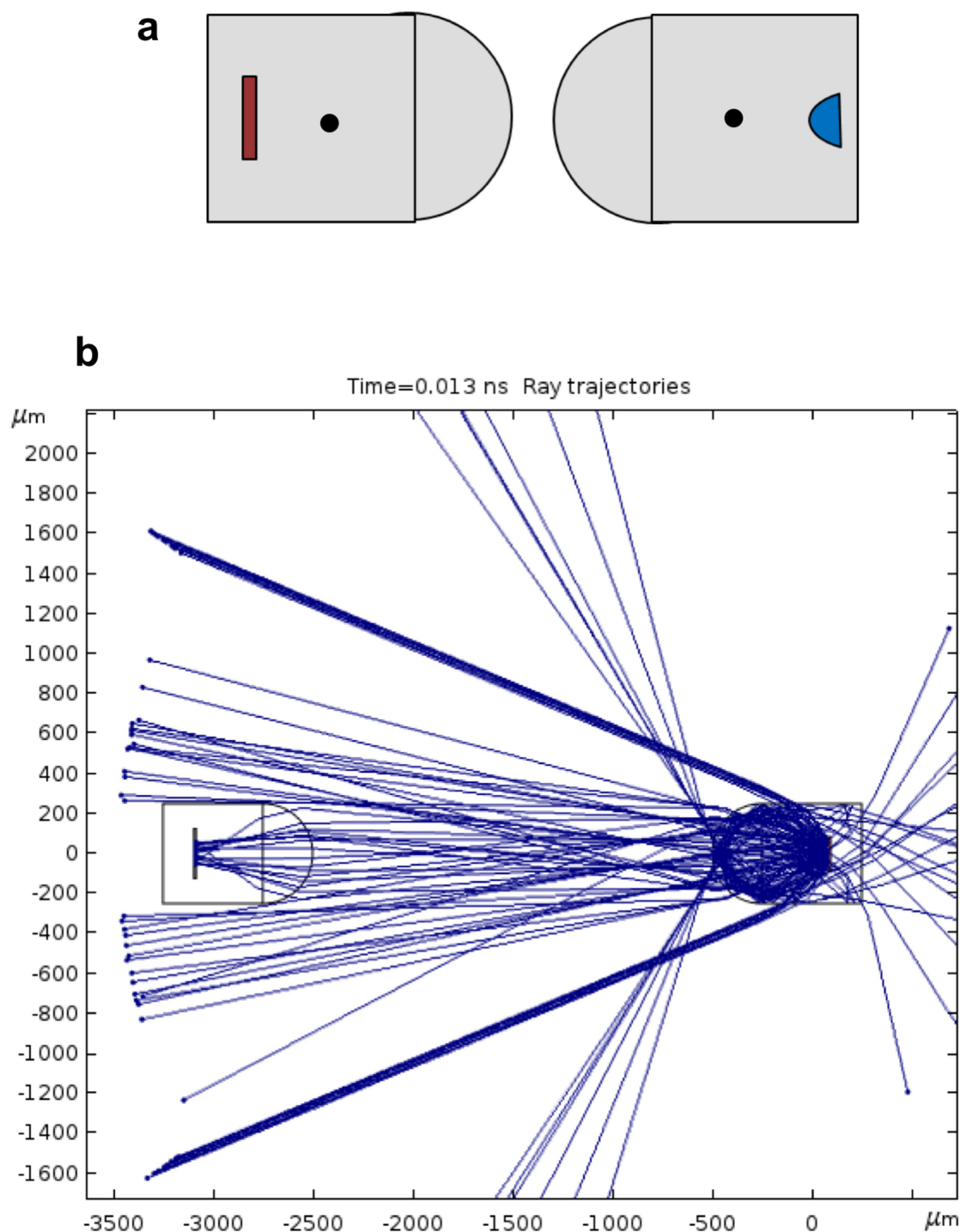
Extended Data Fig. 6 | Simulation of light-emitting fibre structure with a lens. a, Illustration of the fibre structure. Blue, LED; grey, PC cladding. Fibre size, 500 μm × 500 μm. The black dot shows the centre of the fibre. The radiation pattern was assumed to be Lambertian. **b**, Results of the ray-optics simulations, showing collimation of the light from the LED when the device is placed at 190 μm from the centre of the fibre. The fibre structure is outlined by a black curve, and a general photodetector is plotted on the right-hand side of the figure. Blue lines represent optical rays emitted by the LED in the fibre.

a

b

c
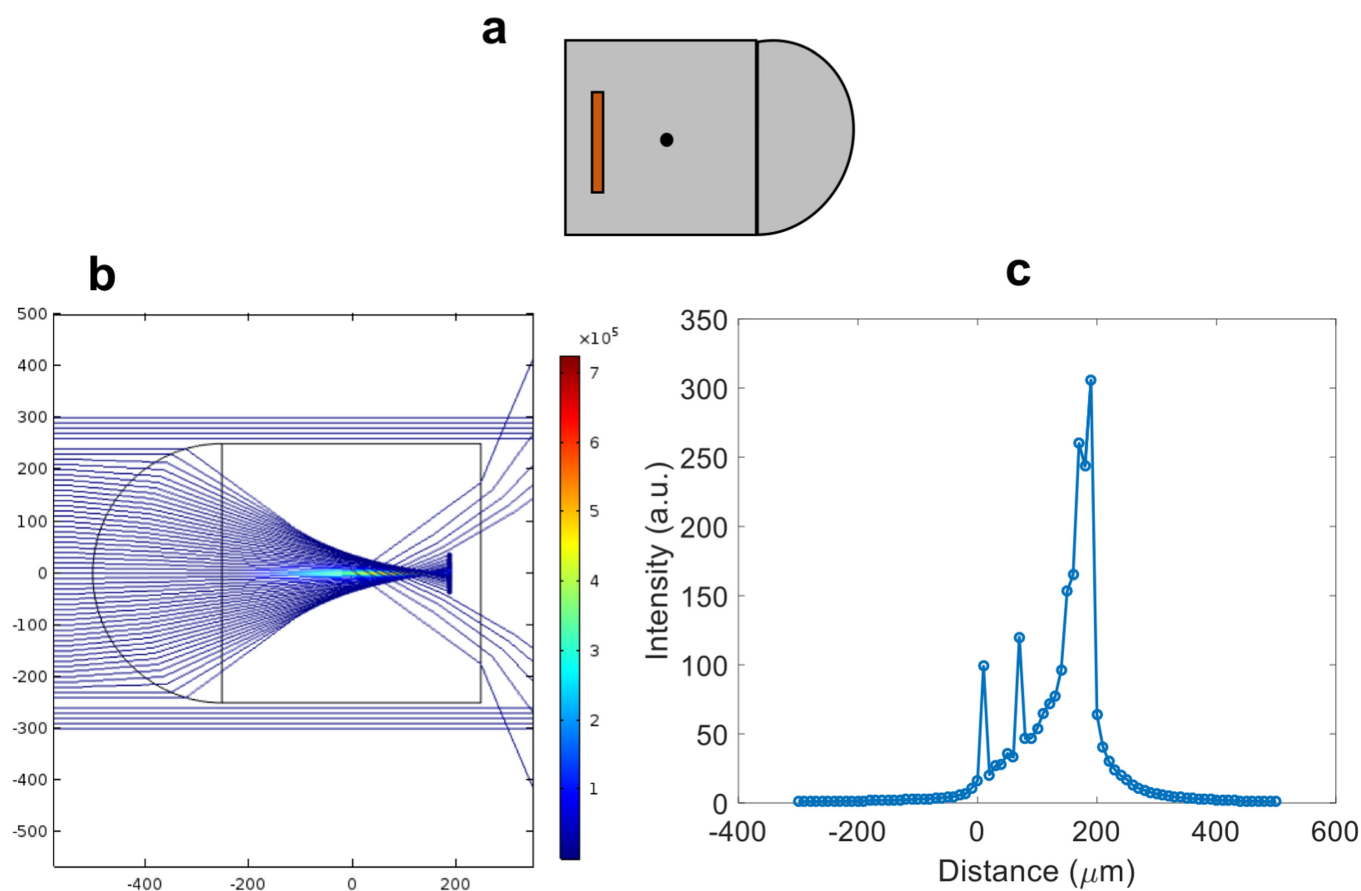
Extended Data Fig. 7 | Simulation of photodetecting fibre structure with a lens. a, Illustration of the fibre structure. Red, photodetector; grey, PC cladding. Fibre size, 500 μm × 500 μm. The centre of the fibre is denoted by a black dot. **b**, Results of the ray-optics simulations, showing focusing of the collimated external light on the photodetecting device.

The results were obtained with the device placed 190 μm away from the centre of the fibre. Axis units, μm. **c**, The intensity of the illumination as a function of the location of the device in the fibre. The maximal intensity is achieved at 190 μm from the centre of the fibre.

Extended Data Fig. 8 | Simulation of a lensed communication system containing a light-emitting fibre and a photodetecting fibre.
a, Illustration of the fibre system structure. Red, photodetector; blue, light-emitting device; grey, PC cladding. Fibre size, 500 μm × 500 μm. The black dot denotes the centre of the fibre. **b**, Results of the ray-optics simulations that show collimation of the emitted light and focusing of the light on the photodetecting device, with the devices placed 190 μm from the centre of the fibre.
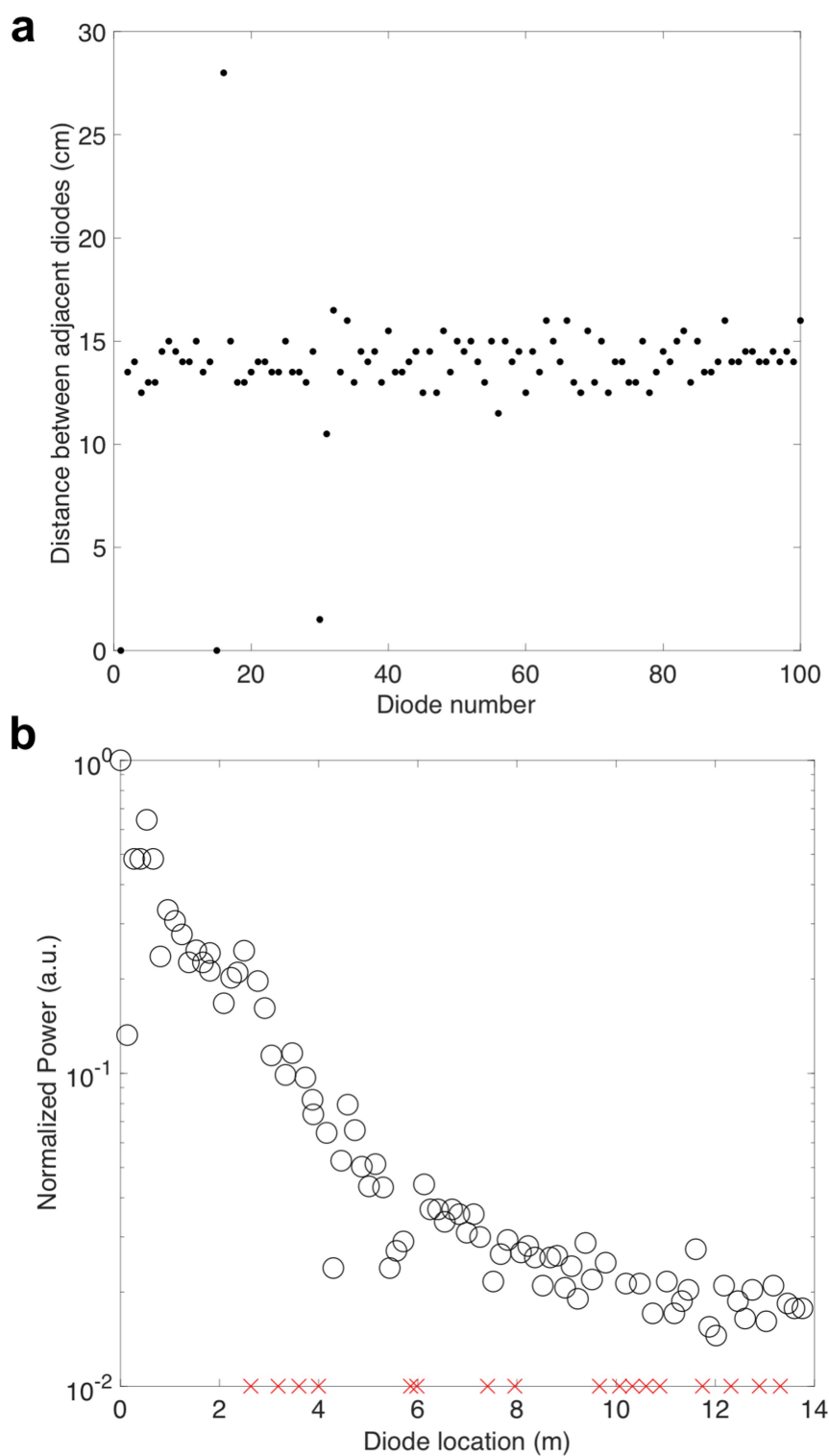
Extended Data Fig. 9 | Characterization of a typical preform draw.
a, Measured distance between adjacent LEDs in the drawn fibres. The diodes were arranged in two parallel arrays in the preform, which was drawn with a draw-down ratio of 33. **b**, Optical power characterization of the LEDs in the drawn fibre. The power was normalized with the power of the brightest diode, which was located adjacent to the power source. Non-operational LEDs are marked by a red cross. The emitted power decays as the voltage drops on the wires in the fibre for devices located away from the power source.